Journal of Photochemistry and Photobiology A: Chemistry 198 (2008) 282–287

Contents lists available at ScienceDirect

Journal of Photochemistry and Photobiology A: Chemistry

journal homepage: www.elsevier.com/locate/jphotochem

Highly photocatalytic activity of metallic hydroxide/titanium dioxide nanoparticles prepared via a modified wet precipitation process

Nan Wang, Jing Li, Lihua Zhu*, Ying Dong, Heqing Tang*

Department of Chemistry and Chemical Engineering, Hubei Key Lab of Bioinorganic Chemistry and Materia Medica, Huazhong University of Science and Technology, 1037 Luo-Yo Road, Hong-shan-qu, Wuhan 430074, China

ARTICLE INFO

Article history:
Received 28 August 2007
Received in revised form
25 November 2007
Accepted 26 March 2008
Available online 16 April 2008

Keywords:
Titanium dioxide
Surface modification
Ferric hydroxide
Cupric hydroxide
Photocatalysis

ABSTRACT

Surface modification is one important approach to increase the photocatalytic activity of TiO_2. By using a modified wet precipitation process, novel $M(OH)_x/TiO_2$ nanoparticles were synthesized, where $M(OH)_x$ represents ferric or cupric hydroxide. The prepared $M(OH)_x/TiO_2$ powders were characterized with XRD, FT-IR, BET, UV–vis DRS, and TGA, and were observed to yield high photocatalytic ability by using methyl orange (MO) as a model compound of organic pollutants to be degraded. Due to the accelerating effects of the new photocatalyst, the half-time of MO during its photocatalytic degradation at pH 6.0 over $M(OH)_x/TiO_2$ was decreased from 332 min for unmodified neat TiO_2 to 63 min for $Fe(OH)_3/TiO_2$ and 65 min for $Cu(OH)_2/TiO_2$, respectively. The enhancing effects of $M(OH)_x/TiO_2$ was further observed in a wide composition range with various M/Ti atomic ratios in the photocatalysts and in a wide pH range of the MO solution from 3 to 7. This enhancing effect is mainly attributed to the increased trapping of the photogenerated electron by the higher valence sites (Fe(III) or Cu(II)) in the hydroxide layer near the $M(OH)_x/TiO_2$ interface and the enriched surface hydroxyl groups which accept photogenerated holes to yield more hydroxyl radicals.

1. Introduction

Increasing attention has been paid to semiconductor photocatalysis for its role in the destruction of environmental toxic pollutants [1–6]. Among the semiconductor catalysts, TiO_2 is the most widely investigated one because of its favorable chemical property, high stability, and low cost. However, the efficient application of TiO_2 is obviously limited due to its narrow absorption wavelength range (only 5% of the spectrum of the incoming sunlight in the near ultraviolet region) and low quantum yields (often <5%). It is well known that improving of the quantum yield of TiO_2-based photocatalysis requires primarily a reduced e^-–h^+ recombination rate, which can be achieved by depositing noble metals on the surface of TiO_2 [1], coupling TiO_2 with other semiconductors [5], and doping with transition metal ions [7–12]. Among these techniques, a lot of works are devoted to doping with iron and copper which act as charge separators of the photo-induced electron–hole pair and consequently enhance the photocatalytic activity of TiO_2 [7]. Chiang reported that the loading 0.10 at.% Cu of copper oxide onto the surface of TiO_2 enhances slightly the photodegradation of cyanide [8]. Wong et al. observed that the Cu-doped TiO_2 nanocatalysts with a low Cu concentration (up to 1% Cu) prepared by the photodeposition method showed enhanced photocatalytic activity, and the TiO_2 nanocatalyst doped with 1% Cu showed the best performance [9]. Besides surface doping, bulk doping was another main interesting study and the bulk doping TiO_2 may be synthesized by sol–gel method [10], co-combustion [11], plasma evaporating [12], but the most used way is a wet impregnation and coprecipitation process [13,14]. Wang et al. improved the wet process by using a mixture of organic Ti and Fe precursors and prepared catalysts with enhanced photocatalytic activity due to the improved uniform distribution of Fe in the TiO_2 matrix [15]. However, in order to obtain uniform bulk doping, the photocatalysts must be heated at rather high temperature [7,14], which is necessary for at least uniform dispersing of Fe or Cu into the TiO_2 matrix, transformation of TiO_2 to an appropriate phase, and/or formation of a porous surface structure.

Recently, we are interested at the improvements of the photocatalytic activity of TiO_2 by surface modification. The effective surface modification of TiO_2 photocatalysts may be achieved by adsorbing a monolayer of special organic compounds [2], by adsorbing in situ inorganic anions and cations (such as F^- and Cu^{2+} [3]), coating a layer of molecularly imprinted polymers [4], and by depositing noble metals on the surface of TiO_2 [1]. In consideration of the effectiveness of doping with transition metal ions [7–12], a new surface modification approach can be derived from the bulky doping

* Corresponding authors. Tel. +86 27 87543432, fax +86 27 87543632.
E-mail addresses: lhzhu63@yahoo.com.cn (L. Zhu), hqtang62@yahoo.com.cn (H. Tang).

1010-6030/$ – see front matter © 2008 Elsevier B.V. All rights reserved.
doi:10.1016/j.jphotochem.2008.03.021

with transition metal ions. Based on the conventional wet impregnation and coprecipitation process [13], therefore, we develop a modified preparation process by omitting the step of calcinations, as an extension of our previous work [2–4,16]. This leads to novel $M(OH)_x/TiO_2$ ($M = Fe^{3+}, Cu^{2+}$) nanoparticles, which may function as a new type of TiO_2 photocatalysts consisting a $M(OH)_x/TiO_2$ interface. By using photocatalytic degradation of a non-biodegradable azo dye methyl orange (MO), the new photocatalysts are confirmed to possess significantly enhanced photocatalytic activity.

2. Experimental

2.1. Materials and photocatalyst preparation

Two types of TiO_2 powders were used as received: one (average particle size 20 nm) was provided by Zhoushan Nano Company, and the other (P25) was provided by Degassa. For simplicity, the first one was referred to as (neat) TiO_2 throughout the present work, in order to be distinguished from the second one (P25). All other chemicals were of analytical reagent grade and used without further purification. Distilled water was used throughout. The pH of solutions was adjusted by using diluted aqueous HCl or $NH_3{\cdot}H_2O$ solutions.

To synthesize the $M(OH)_x/TiO_2$ nanoparticles, 2.0 g of commercial TiO_2 powders and Fe(III) or Cu(II) salt were dispersed in an acidic aqueous solution (pH ≈ 2) by sonicating for 5 min. An aqueous ammonia solution was added dropwise into the mixture suspension to a final pH of 8–9, leading to a coating of ferric or cupric hydroxide on the surface of TiO_2 nanoparticles due to the precipitation of ferric or cupric ions. After being isolated, the obtained powders finally were vacuum dried at 50 °C for 1 h. To easily understand the composition of the new photocatalyst, it is referred to as a name containing the atomic ratio of the used metal (Fe, Cu) and titanium (M/Ti). For example, when a mixture of transition metal ions and neat TiO_2 with a M/Ti atomic ratio of 0.05% is used in the preparation process, the obtained $M(OH)_x/TiO_2$ photocatalyst is referred to as 0.05-$M(OH)_x/TiO_2$. Here, it should be noted that it is unnecessary that the $M(OH)_x/TiO_2$ photocatalysts have a perfect shell–core structure because only such a small amount of $M(OH)_x$ was coated on the surface of TiO_2 particles.

2.2. Photocatalyst characterization

X-ray diffraction (XRD) patterns were obtained on an X'Pert PRO X-ray diffractometer (PANalytical) with a Cu Kα radiation source. FT-IR spectra were recorded on a VERTEX 70 spectrometer (Bruker) in the transmission mode in spectroscopic grade KBr pellets. The low-temperature N_2 adsorption–desorption experiments were carried out using a Quantachrome Autosorb-1 system. All samples were degassed for 3 h at 353 K before the analysis. The specific surface area was calculated using the BET method based on the N_2 adsorption isotherm. UV–visible diffuse reflectance (UV–vis DRS) spectra were recorded at room temperature and in air by means of a UV-2550 spectrometer (Shimadzu) equipped with an integrating sphere attachment using $BaSO_4$ as background. Thermogravimetric analysis (TGA) was carried out on a TGS-2 instrument (PerkinElmer) at a heating rate of 10 °C min^{-1} in air.

2.3. Photocatalytic experiment

By using MO as a model pollutant, its photocatalytic degradation was performed in a 400 mL quartz reactor, being filled with 250 mL of aqueous suspension containing catalyst (1 g L^{-1}) and MO (10 mg L^{-1}). The mixture suspension was stirred continuously for 20 min before being illuminated, to favor the organic adsorption onto the catalyst surface. A 250 W high-pressure mercury lamp (Philips) was employed as a UV light source. At given time intervals, 2 mL aliquots were sampled, immediately centrifuged at 14000 rpm for 15 min to remove the TiO_2 nanoparticles, and then analyzed on a Cary 50 UV–visible spectrophotometer (Varian) by measuring the absorbance of the solution at 464 or 504 nm, which corresponds to the maximum absorption of MO in neutral or acidic solutions, respectively.

3. Results and discussion

3.1. Enhanced photocatalytic activity of $M(OH)_x/TiO_2$ nanoparticles

In control experiments, we confirmed that the disappearance of MO was negligible when the MO solution is not irradiated with UV light or no TiO_2 photocatalyst was added into the solution. The photocatalytic degradation of MO only occurred over TiO_2 under UV light illumination. Fig. 1 illustrates the kinetics of MO degradation over different TiO_2 photocatalysts. The MO photodegradation over neat TiO_2 is very slow, proceeding with a kinetic behavior of pseudo-first-order reaction as $\ln(c/c_0) = k_1 t + m$ (curve 1). Here, c_0 and c represent the initial and the remained MO concentrations, k_1 is the rate constant of the pseudo-first-order reaction, t is the illumination time (min), and m is a constant. The rate constant k_1 was found to be dependent on the initial MO concentration and the initial solution pH value. This kinetic behavior of pseudo-first-order reaction is well consistent with the results reported for the photocatalytic degradation of MO over TiO_2 and conventional Fe-doped TiO_2 in the literature [17,18]. For $c_0 = 10$ mg L^{-1} and pH 6.0, the kinetics was fitted as $\ln(c/c_0) = -0.00209t - 0.0418$ (regression coefficient, $R = 0.997$).

However, it is easily understood from Fig. 1 that the rate of MO degradation is significantly enhanced over the as-prepared 0.05-$M(OH)_x/TiO_2$ catalyst, following a pseudo-zero-order rate equation of $c/c_0 = k_0 t + n$ (curves 2 and 3 in Fig. 1), where both k_0 and n are constants. The rate constant k_0 was found to be dependent on the initial MO concentration and the initial solution pH value. Under the conditions of $c_0 = 10$ mg L^{-1} and pH 6.0, the kinetics over 0.05-$Fe(OH)_3/TiO_2$ and 0.05-$Cu(OH)_2/TiO_2$ catalyst were fitted as $c/c_0 = -0.00782t + 0.992$ ($R = 0.999$) and $c/c_0 = -0.00716t + 0.962$ ($R = 0.996$), respectively.

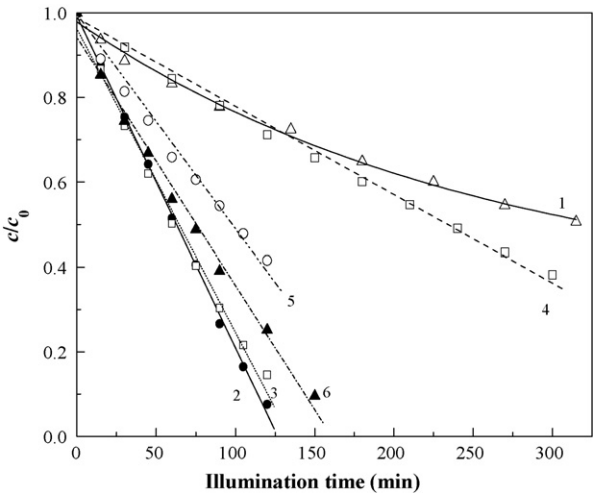

Fig. 1. Kinetics of MO degradation (10 mg L^{-1}, pH 6) over (1) TiO_2, (2) 0.05-$Fe(OH)_3/TiO_2$, (3) 0.05-$Cu(OH)_2/TiO_2$, (4) 0.05-$Fe(OH)_3/TiO_2$ annealed at 250 °C for 120 min, (5) 0.05-$Cu(OH)_2/TiO_2$ annealed at 250 °C for 120 min, and (6) P25.

The photocatalytic ability of the $M(OH)_x/TiO_2$ catalysts was found to be influenced by several factors such as the nominal content of metal ions and the solution pH. To compare the photocatalytic ability of the $M(OH)_x/TiO_2$ composites with that of neat TiO_2, we will use the half-time ($t_{1/2}$) of MO (the time required for one-half of MO to be degraded), because of the different dimensions of the rate constants k_0 and k_1. For example, for a given 10 mg L^{-1} MO solutions and given pH of 6.0, the value of $t_{1/2}$ for neat TiO_2 was 332 min, whereas $M(OH)_x$ deposition increased the rate of MO degradation and $t_{1/2}$ was decreased to 63 min for 0.05-$Fe(OH)_3/TiO_2$ and 65 min for 0.05-$Cu(OH)_2/TiO_2$, respectively, being smaller than 73 min over P25 (curve 6 in Fig. 1). This indicates that the $M(OH)_x$ deposition accelerates the photocatalytic degradation of MO by about five times, showing photocatalytic ability as excellent as Degussa P25, a well-studied and highly efficient photocatalyst as a control.

3.2. Effect of the chemical composition of $M(OH)_x/TiO_2$

The chemical composition of a catalyst often strongly influences its catalytic performances. The chemical composition of $M(OH)_x/TiO_2$ photocatalysts can be varied by changing the concentrations of cupric or ferric salt used in the preparation process. Here, the nominal chemical composition of $M(OH)_x/TiO_2$ photocatalysts is represented by the atomic ratio of M/Ti in the preparation solution, which in fact reflects the average thickness of the $M(OH)_x$ layer coated on the surface of TiO_2 nanoparticles. By using $M(OH)_x/TiO_2$ photocatalysts with different M/Ti atomic ratios, the photocatalytic degradation of MO was carried out in solutions containing 10 mg L^{-1} MO and 1 g L^{-1} photocatalyst at pH 6.0. As demonstrated in Fig. 2, $t_{1/2}$ decreases markedly by a factor of about five when a little amount of $M(OH)_x$ is deposited on neat TiO_2 particles. The enhanced photocatalytic activity can persist for a fairly wide range of nominal M/Ti atomic ratios from about 0.02% to 0.4% for $Fe(OH)_3/TiO_2$, and from 0.02% to 0.2% for $Cu(OH)_2/TiO_2$, respectively. As the nominal M/Ti atomic ratio goes on increasing, $t_{1/2}$ increases to an extent, indicating that a over thick layer of $M(OH)_x$ is unfavorable to the photocatalytic activity of the photocatalyst.

3.3. Effect of photocatalyst load

Generally, photocatalytic degradation of organic substrates is promoted as the load of TiO_2 photocatalysts is increased. This was also similarly observed for $M(OH)_x/TiO_2$ composite catalysts. In the case of 0.05-$M(OH)_x/TiO_2$, the effect of photocatalyst load is shown in Fig. 3. As the photocatalyst load is increased from 0.5 to 2.0 g L^{-1}, the rate constant k_0 is linearly increased, resulting in a decreasing of $t_{1/2}$ from 93 to 47 min. However, the value of $t_{1/2}$ almost does not change or increases slight when the photocatalyst load is beyond 2.0 g L^{-1}, due to the shadowing effect, wherein the high TiO_2 concentration decreases the penetration depth of UV radiation.

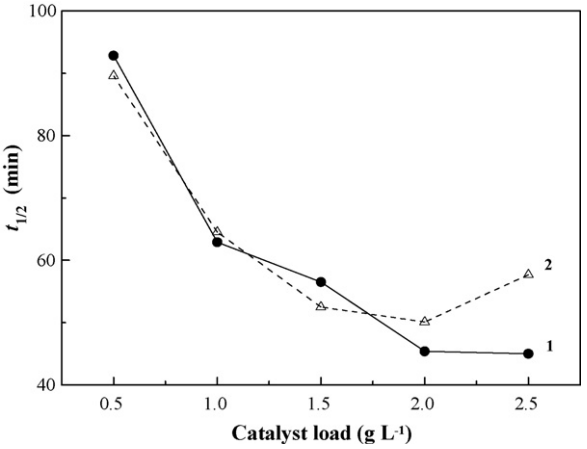

Fig. 3. Effects of catalyst load of (1) 0.05-$Fe(OH)_3/TiO_2$ and (2) 0.05-$Cu(OH)_2/TiO_2$ on $t_{1/2}$ of MO degraded in 10 mg L^{-1} MO solutions at pH 6.

3.4. Effect of pH

The dependence of $t_{1/2}$ on solution pH value was measured as shown in Fig. 4. For a given initial MO concentration of 10 mg L^{-1}, the time $t_{1/2}$ over different photocatalysts almost did not vary as solution pH was increased from pH 3 to 5. When pH was increase beyond pH 5.0, $t_{1/2}$ over neat TiO_2 drastically increased (curve 1). However, the 0.05-$M(OH)_x/TiO_2$ composite catalyst kept small $t_{1/2}$ value until pH 6.0, and showed a rather small increasing of $t_{1/2}$ at pH 7.0 (curves 2 and 3). This demonstrates that the $Fe(OH)_3$ or $Cu(OH)_2$ coating promotes significantly the photocatalytic ability of TiO_2 in weakly acidic and neutral solutions.

It is well known that adsorption of an organic pollutant on the photocatalyst takes an important role in the degradation of the pollutants. Hence, it is necessary to check the effect of $M(OH)_x$ deposition on the MO adsorption. To evaluate the adsorption of MO

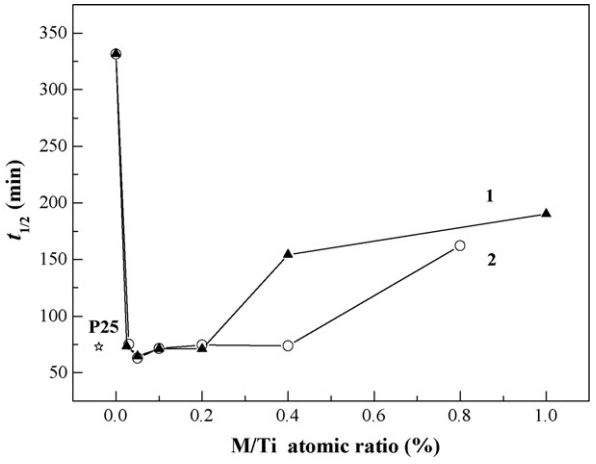

Fig. 2. Effect of M/Ti atomic ratio in $M(OH)_x/TiO_2$ photocatalysts on $t_{1/2}$ of MO degradation in 10 mg L^{-1} MO solutions at pH 6 over 1 g L^{-1} photocatalyst of (1) $Fe(OH)_3/TiO_2$ and (2) $Cu(OH)_2/TiO_2$. As a control, $t_{1/2}$ = 73 min over P25.

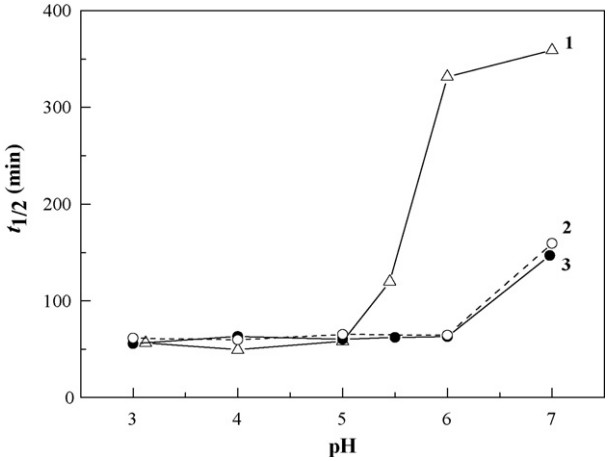

Fig. 4. Dependence of $t_{1/2}$ on pH in solutions of 10 mg L^{-1} MO in the presence of 1 g L^{-1} of (1) neat TiO_2, (2) 0.05-$Cu(OH)_2/TiO_2$ and (3) 0.05-$Fe(OH)_3/TiO_2$.

Table 1
Saturated adsorption of MO (10 mg L^{-1}) on different photocatalysts

Solution pH	Adsorption on photocatalyst (mg g^{-1})		
	Neat TiO_2	0.05-$Fe(OH)_3/TiO_2$	0.05-$Cu(OH)_2/TiO_2$
3	1.50	0.53	0.81
4	1.19	0.31	0.46
5	0.50	0.28	0.35
6	0.05	0.20	0.22
7	0.05	0.07	0.05

on different photocatalyst, 0.22 g of the photocatalyst was added into 110 mL of 10 mg L^{-1} MO solution, the pH value of which was adjusted with dilute HCl and ammonia water. The mixture was well stirred for 2 h in the dark, followed by a high speed centrifuging. From the remaining concentration of MO in the supernatant, the adsorption amount of MO was calculated as saturated adsorption of MO on different catalysts. Table 1 illustrates the dependence of saturated adsorption of MO on different catalysts at various pH values. By comparing the saturated adsorption and the value of $t_{1/2}$ over these three catalysts at different pH values, we can find that in the pH range from 3 to 5, these three catalysts provide almost the same photocatalytic ability (Fig. 4), though the saturated MO adsorption on neat TiO_2 is much higher than that on 0.05-$M(OH)_x/TiO_2$. In the pH range from 5.5 to 7.0, however, 0.05-$M(OH)_x/TiO_2$ yields significantly greater photocatalytic ability than neat TiO_2, though the saturated MO adsorption on these catalysts are close to each other. These results hint that the enhanced photocatalytic activity should not be substantially due to the possible enhancement of adsorption.

To explain the higher photocatalytic activity of $M(OH)_x/TiO_2$ nanoparticles, we tried to correlate the photocatalytic activity and characterization results such as XRD, FT-IR and TGA measurements for the photocatalyst. The detected XRD patterns indicate that both the neat TiO_2 and $M(OH)_x/TiO_2$ particles possessed a crystalline anatase lattice structure. We could not observe any peaks arisen from iron (or copper) species, due to the quite low content of iron or copper in the 0.05-$M(OH)_x/TiO_2$ particles. By using Scherrer equation [19], the average diameter of the 0.05-$Fe(OH)_3/TiO_2$ and 0.05-$Cu(OH)_2/TiO_2$ particles was calculated as 21, 20 nm, respectively, being almost the same as the neat TiO_2, due to the very limited deposition of the ferric hydroxide or copper hydroxide deposition on the surface of TiO_2. BET surface area of the catalysts was measured, respectively as 180.9 m^2 g^{-1} for neat TiO_2 and 121.6–187.0 m^2 g^{-1} for $M(OH)_x/TiO_2$, depending on nominal M/Ti atomic ratio in the catalysts. The $M(OH)_x/TiO_2$ composites tended to have a smaller BET surface area than the neat TiO_2, due to possible aggregation of the nanoparticles.

UV–visible diffuse reflectance spectra of neat TiO_2 and the $M(OH)_x/TiO_2$ composites were measured as shown in Fig. 5. Compared with the neat TiO_2, the over-coating of $Fe(OH)_3$ or $Cu(OH)_2$ makes the absorption edge shift slightly to longer wavelengths, accompanied by a small increase of absorption in the visible light region. There is almost no change in the UV–vis DRS of neat TiO_2 after 0.05% $M(OH)_x$ deposition, hence, the reason for enhanced photocatalytic activity is not due to the change of UV energy absorption.

It is worthy noting that surface hydroxyl groups take an important role in the photocatalytic process on TiO_2 catalysts, which is ascribed to that these groups accept photogenerated holes to form hydroxyl radicals thus preventing electron-hole recombination [20,21]. The FT-IR and TGA studies were measured to confirm the surface hydroxyl groups on the $M(OH)_x/TiO_2$ nanoparticles. Fig. 6 illustrated the FT-IR spectra of neat TiO_2 and $M(OH)_x/TiO_2$ nanoparticles. For neat TiO_2 (curve 1 in Fig. 6), a broad band at 3500–3000 cm^{-1} is assigned to the coordinated water molecules with hydrogen bonds, and the 1622 cm^{-1}-band is assigned to the

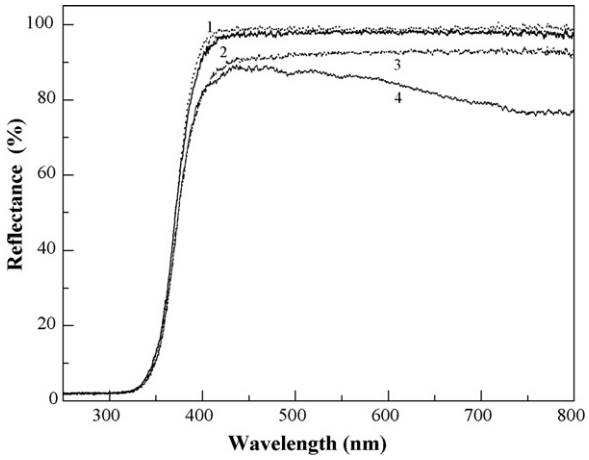

Fig. 5. UV–vis diffuse reflectance spectra of (1) neat TiO_2, (2) 0.05-$Fe(OH)_3/TiO_2$, (3) 0.2-$Fe(OH)_3/TiO_2$ and (4) 0.2-$Cu(OH)_2/TiO_2$ composites.

bending mode of the adsorbed water molecules. These assignments are slightly different from that reported by Gao et al. [22]. Because the surface of TiO_2 is covered with the water molecules, we could not observe the stretching bands in the range from 3750 to 3600 cm^{-1} and the bending mode in low frequency regions around 800–500 cm^{-1} for free Ti-OH groups. The absorption peak at 1405 cm^{-1}, being similar to that at 1409 cm^{-1} observed for freshly prepared TiO_2 powder by a wet process, is still hardly assigned. This peak should not arise from the organic contaminates or carbonate ions adsorbed on the surfaces, because no any organic compounds and carbonates were used in the preparation of the $M(OH)_x/TiO_2$ photocatalysts. Thus, this band may be related to the coordinated H_2O or surface hydroxyls. Compared with the spectrum of neat TiO_2, the bands at 1405 and 3150 cm^{-1} are slightly in strength in the $Cu(OH)_2/TiO_2$ composite (curve 3 in Fig. 6), and these two bands are markedly increased in the $Fe(OH)_3/TiO_2$ (curve 2 in Fig. 6). Furthermore, the bands at 3150 cm^{-1} shifted to lower wavenumbers by about 20 cm^{-1}. These suggest that there are more coordinated H_2O or surface hydroxyls bounded on the surface of the $M(OH)_x/TiO_2$ particles with stronger chemical bonding, especially on the $Fe(OH)_3/TiO_2$. When the nanoparticles are heated at 250 °C for 120 min, the $M(OH)_x$ coating will be converted to a M_xO_y coating, and consequently these two absorption bands are weaken significantly in strength (curves 4 and 5 in Fig. 6).

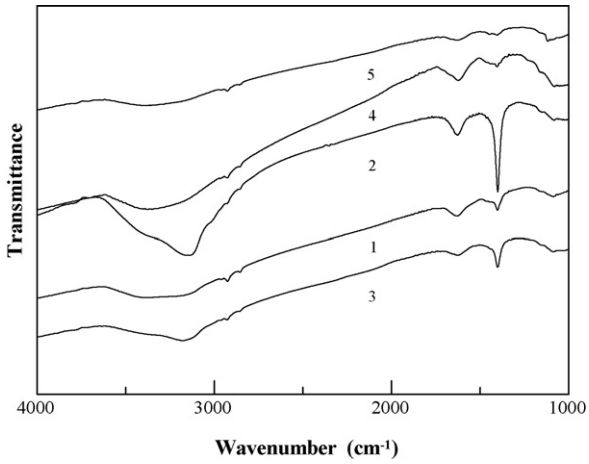

Fig. 6. FT-IR spectra of (1) TiO_2, (2) 0.05-$Fe(OH)_3/TiO_2$, (3) 0.05-$Cu(OH)_2/TiO_2$, (4) 0.05-$Fe(OH)_3/TiO_2$ heated at 250 °C for 120 min, and (5) 0.05-$Cu(OH)_2/TiO_2$ heated at 250 °C for 120 min.

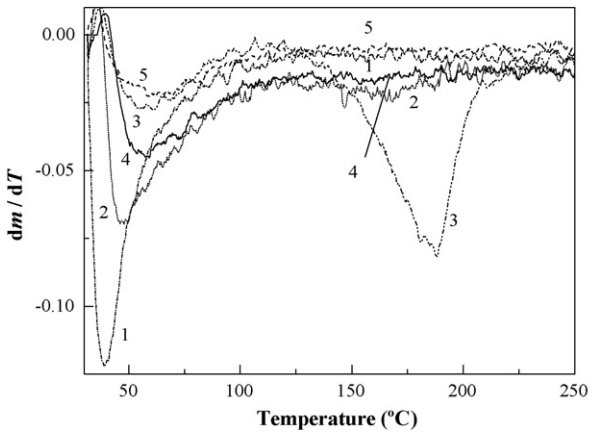

Fig. 7. DTG curves of (1) TiO_2, (2) 0.05-$Cu(OH)_2/TiO_2$, (3) 0.05-$Fe(OH)_3/TiO_2$, (4) 0.05-$Cu(OH)_2/TiO_2$ heated at 250 °C for 120 min, and (5) 0.05-$Fe(OH)_3/TiO_2$ heated at 250 °C for 120 min.

The TGA study also confirmed that the $M(OH)_x/TiO_2$ bounded larger surface hydroxyls or coordinated H_2O as shown in Fig. 7. The DTG curve of neat TiO_2 (curve 1 in Fig. 7) shows an endothermic peak at about 50 °C, due to the loss of loosely bound water. Compared with neat TiO_2, the $Cu(OH)_2/TiO_2$ shows a broader peak from room temperature to ca. 100 °C, due to the desorption of loosely bound and coordinated water because the $Cu(OH)_2$ coating will be converted to a CuO coating at 100 °C. Whereas the $Fe(OH)_3/TiO_2$ nanoparticles yield a peak over the range from 150 to 240 °C (curve 3 in Fig. 7), which is ascribed to the loss of coordinated H_2O or surface hydroxyls bounded on the surface of the particles with stronger chemical bonding. When the $M(OH)_x/TiO_2$ composite is annealed at 250 °C for 2 h, the peak from room temperature to 100 °C for $Cu(OH)_2/TiO_2$ is weaken significantly (curve 4 in Fig. 7) and the peak over the range from 150 to 240 °C for $Fe(OH)_3/TiO_2$ disappears completely (curve 5 in Fig. 7), behaving like the neat TiO_2 without the coating of $M(OH)_x$.

From the TGA and FT-IR studies, the amount of surface hydroxyls or coordinated H_2O is observed to increase in the order of neat TiO_2 < $Cu(OH)_2/TiO_2$ < $Fe(OH)_3/TiO_2$. After heat-treatment at 250 °C for 2 h, the $M(OH)_x/TiO_2$ lost the surface hydroxyl groups and coordinated H_2O, as expected, the enhancing effect of the $M(OH)_x$-deposited catalyst was lost to a certain extent (curves 4 and 5 in Fig. 1), especially, the enhancing effect of the $Fe(OH)_3$-deposited catalyst was lost almost completely (curve 4 in Fig. 1). This suggests the increased surface hydroxyl groups or coordinated H_2O due to the $M(OH)_x$ coating is very important to the enhanced photocatalytic activity of $M(OH)_x/TiO_2$ nanoparticles. The coordinated water and/or surface hydroxyl radicals may enhance the photo-reduction of O_2 to O_2^-, which can further disproportionate into H_2O_2, resulting in the promoted formation of hydroxyl radicals.

It is interesting to note that the 0.05-$M(OH)_x/TiO_2$ after heat-treatment show higher photocatalytic activity than neat TiO_2, especially for 0.05-$Cu(OH)_2/TiO_2$ (curve 5 in Fig. 1), indicating that the reason for enhanced activity is not only due to large amount of hydroxyl species, but also due to other aspects. Another important reason for such a high activity can be attributed to the interface between $M(OH)_x$ and TiO_2, near which the higher valence sites (Fe(III) or Cu(II)) in the hydroxide layer may increase the trapping of the photogenerated electron. It has been reported that a p–n junction in a composite photocatalyst will yield a driving force for the transport of photogenerated charge carriers [23,24]. In our case, a similar hetero-junction effect is possibly considered, although it is not a real p–n junction. At the region near the $M(OH)_x/TiO_2$ interface, the photo-induced electrons in the conduction band of TiO_2 will immediately flow to the side of $M(OH)_x$ and are trapped by the higher valence sites due to the reduction of the higher valence species ($Fe^{3+} + e^- \rightarrow Fe^{2+}$; $Cu^{2+} + e^- \rightarrow Cu^+$). In this way, the recombination of the electron-hole pairs is suppressed, and the $M(OH)_x/TiO_2$ interface consequently may improve the photocatalytic activity. In addition, the resulting Fe^{2+} or Cu^+ initiates the Fenton reaction, resulting in acceleration of OH radicals generation to an extent.

Maintaining high activity in weakly acidic and neutral solutions is an important merit of the $M(OH)_x/TiO_2$ nanoparticles as photocatalyst. Homogeneous and heterogeneous photo-Fenton reactions have found wide applications in discoloration and mineralization of azo dyes, which requires an optimal solution pH of about pH 3.0 for the optimal photocatalytic activity [25]. It is also reported that the rate and extent of photocatalytic oxidation of organic pollutants can achieve a maximum at about pH 3.0 in UV/TiO_2 system [26]. However, the novel $M(OH)_x/TiO_2$ composite particles can perform efficiently over a wide pH range, at least from pH 3 to 7. For the treatment of industrial wastewaters, hence, it is unnecessary to pre-adjust the pH values of the wastewaters to obtain high photocatalytic efficiency.

3.5. Duration of the $M(OH)_x/TiO_2$ photocatalyst

To evaluate the stability of the new photocatalysts, the photocatalytic degradation of 10 mg L^{-1} MO at pH 6.0 was carried out in successive batches. After the added MO was almost completely degraded in the first run, 10 mg L^{-1} of MO was freshly added and then the second photodegradation cycle started. This process was repeated for six cycles of the photocatalytic degradation. For the 0.05-$Fe(OH)_3/TiO_2$ nanocomposites, presented in Fig. 8, each section of the c/c_0–t curve corresponding to a degradation cycle is very close to curve 2 in Fig. 1, behaving as a pseudo-zero-order reaction in kinetics. By fitting the experimental data in Fig. 8, the rate equation for the MO photodegradation was expressed as $c/c_0 = -(0.00775 \pm 0.00028)t + (0.962 \pm 0.014)$ for the six degradation cycles. Similar phenomenon was also observed over the 0.05-$Cu(OH)_2/TiO_2$ photocatalyst. The almost same kinetic behaviors of the degradation process in the cycles demonstrate that the $M(OH)_x/TiO_2$ composite catalyst have an excellent photochemical stability.

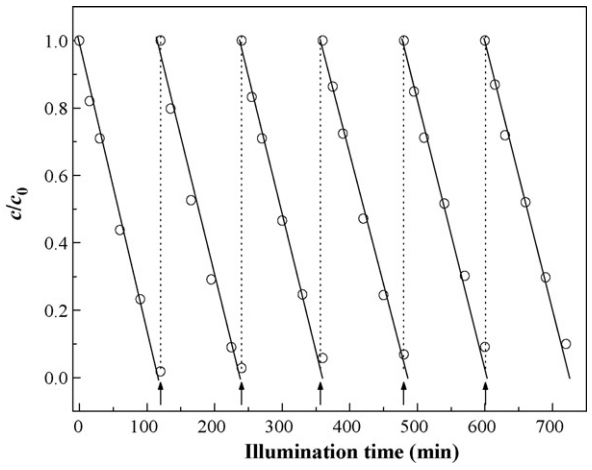

Fig. 8. Kinetics of MO degradation over 0.05–$Fe(OH)_3/TiO_2$ in successive degradation cycles. The arrows indicate the start of a new cycle of degradation after the concentration of MO is replenished to 10 mg L^{-1} in the reaction suspension.

4. Conclusions

We have prepared novel $M(OH)_x/TiO_2$ nanoparticles via a simple synthesis approach at low temperature. By using XRD, UV–vis DRS, TGA, and FT-IR techniques, these composites were characterized as nanoparticles with enriched surface hydroxyls and coordinated water. These composites yielded a strong photocatalytic activity toward the degradation of MO in aqueous solution. Compared with neat TiO_2 without the modification, the photocatalytic activity of 0.05-$M(OH)_x/TiO_2$ was increased by about fivefolds. The most important merits of these new photocatalysts include outstanding photocatalytic activity in a wide pH range from about 3 to 7, easiness of preparation, and excellent photochemical stability. It has been confirmed that the enhanced effect of $M(OH)_x$ deposition is not due to its effect on the MO adsorption, but attributed to the enriched surface hydroxyl groups and the interface of $M(OH)_x/TiO_2$ promoting the charge separation.

Acknowledgements

Financial supports from the National Natural Science Foundation of China (Nos. 30571536 and 20677019) are gratefully acknowledged. The Center of Analysis and Testing of Huazhong University of Science and Technology is thanked for characterization and analysis.

References

[1] D. Hufschmidt, D. Bahnemann, J.J. Testa, C.A. Emilio, M.I. Litter, J. Photochem. Photobiol. A: Chem. 148 (2002) 223–231.
[2] J. Li, L. Zhu, Y. Wu, Y. Harima, A. Zhang, H. Tang, Polymer 47 (2006) 7361–7367.
[3] N. Wang, Z. Chen, L. Zhu, X. Jiang, B. Lv, H. Tang, J. Photochem. Photobiol. A: Chem. 191 (2007) 193–200.
[4] X. Shen, L. Zhu, J. Li, H. Tang, Chem. Commun. (2007) 1163–1165.
[5] J.S. Jang, S.M. Ji, S.W. Bae, H.C. Son, J.S. Lee, J. Photochem. Photobiol. A: Chem. 188 (2007) 112–119.
[6] L. Wang, N. Wang, L. Zhu, H. Yu, H. Tang, J. Hazard. Mater. 152 (2008) 93–99.
[7] A. Di Paola, E. García-López, G. Marcì, C. Martín, L. Palmisano, V. Rives, A.M. Venezia, Appl. Catal. B Environ. 48 (2004) 223–233.
[8] K. Chiang, R. Amal, T. Tran, Adv. Environ. Res. 6 (2002) 471–485.
[9] R.S.K. Wong, J. Feng, X. Hu, P.L. Yue, J. Environ. Sci. Health A 39 (2004) 2583–2595.
[10] J. Zhua, F. Chen, J. Zhang, H. Chen, M. Anpo, J. Photochem. Photobiol. A: Chem. 180 (2006) 196–204.
[11] B. Neppolian, H.S. Jie, J.P. Ahn, J.-K. Park, M. Anpo, Chem. Lett. 33 (2004) 1562–1563.
[12] X.H. Wang, J.G. Li, H. Kamiyama, M. Katada, N. Ohashi, Y. Moriyoshi, T. Ishigaki, J. Am. Chem. Soc. 127 (2005) 10982–10990.
[13] K.T. Ranjit, B. Viswanathan, J. Photochem. Photobiol. A: Chem. 108 (1997) 79–84.
[14] M.I. Litter, J.A. Navfo, J. Photochem. Photobiol. A: Chem. 98 (1996) 171–181.
[15] C.-Y. Wang, C. Böttcher, D.W. Bahnemann, J.K. Dohrmann, J. Mater. Chem. 13 (2003) 2322–2329.
[16] N. Wang, L. Zhu, J. Li, H. Tang, Chin. Chem. Lett. 18 (2007) 1261–1264.
[17] S. Al-Qaradawi, S.R. Salman, J. Photochem. Photobiol. A: Chem. 148 (2002) 161–168.
[18] R.S. Sonawane, B.B. Kale, M.K. Dongare, Mater. Chem. Phys. 85 (2004) 52–57.
[19] K. Nagaveni, G. Sivalingam, M.S. Hegde, G. Madras, Appl. Catal. B Environ. 48 (2004) 83–93.
[20] K. Nagaveni, M.S. Hegde, N. Ravishankar, G.N. Subbanna, G. Madras, Langmuir 20 (2004) 2900–2907.
[21] Z. Ding, G.Q. Lu, P.F. Greenfield, J. Phys. Chem. B 104 (2000) 4815–4820.
[22] Y. Gao, Y. Masude, K. Koumoto, Chem. Mater. 16 (2004) 1062–1067.
[23] Y. Chen, J.C. Crittenden, S. Hackney, L. Sutter, D.W. Hand, Environ. Sci. Technol. 39 (2005) 1201–1208.
[24] R. Brahimi, Y. Bessekhouad, A. Bouguelia, M. Trari, J. Photochem. Photobiol. A: Chem. 186 (2007) 242–247.
[25] K. Wu, Y. Xie, J. Zhao, H. Hidaka, J. Mol. Catal. A 144 (1999) 77–84.
[26] P.A. Pekakis, N.P. Xekoukoulotakis, D. Mantzavinos, Water Res. 40 (2006) 1276–1286.